Atmos. Meas. Tech., 3, 1519–1531, 2010
www.atmos-meas-tech.net/3/1519/2010/
doi:10.5194/amt-3-1519-2010


Atmospheric Measurement Techniques

# Field intercomparison of two optical analyzers for $CH_4$ eddy covariance flux measurements

**B. Tuzson[1], R. V. Hiller[2], K. Zeyer[1], W. Eugster[2], A. Neftel[3], C. Ammann[3], and L. Emmenegger[1]**

[1]Empa, Swiss Federal Laboratories for Materials Science and Technology, Laboratory for Air Pollution and Environmental Technology, Überlandstr. 129, 8600 Dübendorf, Switzerland
[2]ETH Zurich, Institute of Plant, Animal and Agroecosystem Sciences, Universitätsstr. 2, 8092 Zürich, Switzerland
[3]Agroscope Reckenholz-Tänikon Research Station ART, Reckenholzstr. 191, 8046 Zürich, Switzerland

Received: 10 June 2010 – Published in Atmos. Meas. Tech. Discuss.: 13 July 2010
Revised: 23 September 2010 – Accepted: 1 November 2010 – Published: 8 November 2010

**Abstract.** Fast response optical analyzers based on laser absorption spectroscopy are the preferred tools to measure field-scale mixing ratios and fluxes of a range of trace gases. Several state-of-the-art instruments have become commercially available and are gaining in popularity. This paper aims for a critical field evaluation and intercomparison of two compact, cryogen-free and fast response instruments: a quantum cascade laser based absorption spectrometer from Aerodyne Research, Inc., and an off-axis integrated cavity output spectrometer from Los Gatos Research, Inc. In this paper, both analyzers are characterized with respect to precision, accuracy, response time and also their sensitivity to water vapour. The instruments were tested in a field campaign to assess their behaviour under various meteorological conditions. The instrument's suitability for eddy covariance flux measurements was evaluated by applying an artificial flux of $CH_4$ generated above a managed grassland with otherwise very low methane exchange. This allowed an independent verification of the flux measurements accuracy, including the overall eddy covariance setup and data treatment. The retrieved fluxes were in good agreement with the known artificial emission flux, which is more than satisfactory, given that the analyzers were attached to separate sonic anemometers placed on individual eddy towers with different data acquisition systems but similar data treatment that are specific to the best practice used by the involved research teams.

*Correspondence to:* B. Tuzson
(bela.tuzson@empa.ch)

## 1 Introduction

Understanding the temporal dynamics of methane emission at the global scale requires continuous and long-term field measurements of $CH_4$ fluxes at representative sites, where the relationships between landscape-scale flux measurements and their environmental drivers can be investigated (Bartlett and Harriss, 1993; Bubier and Moore, 1994). The well established chamber technique, however, poorly captures the spatial and temporal variability of gas exchange despite its undebated usefulness for small scale (plot-level) studies. The general problems associated with chamber flux measurements are leaks, inhibition of fluxes through concentration build-up and pressure effects, which are well known limitations of this method (Matthias et al., 1978; Bain et al., 2005; Camarda et al., 2009). Alternatively, micrometeorological methods like eddy covariance (EC) integrate trace gas exchange over extended areas (typically hundreds of $m^2$) – appropriate for landscape scale studies. However, these techniques rely on fast response, field-deployable and high-sensitivity instruments, which can rapidly resolve small (preferably better than 0.1%) concentration changes in $CH_4$ at ambient level. Until recently, EC flux measurements of $CH_4$ required frequent re-calibration and/or liquid nitrogen for the analyzers (Verma et al., 1992; Fowler et al., 1995; Friborg et al., 1997; Werle and Kormann, 2001) leading to logistic limitations for unattended field deployment.

Recently, a number of new instruments appeared on the market, which may overcome these shortcomings. However, just a very few studies have addressed their application in the field for EC flux measurements and they focus on only one single type of analyzer (Eugster et al., 2007; Eugster and Plüss, 2010; Neftel et al., 2007; Kroon et al., 2007; Hendriks et al., 2008; Smeets et al., 2009). For novel instruments, it is

**Table 1.** Characteristics of the two EC flux systems and respective analyzers.

| Parameters | EC system with FMA | EC system with QCLAS |
|---|---|---|
| Analyzer Type | off-axis integrated cavity output spectrometer | dual cw quantum cascade laser direct absorption spectrometer |
| Measured species | $CH_4$ | $CH_4$; $H_2O$; $N_2O$; $NO_2$ |
| $CH_4$ absorption line position (μm) | 1.65 | 7.84 |
| $CH_4$ line intensity ($\times 10^{-21}$ $cm^{-1}$/molecule $cm^{-2}$) | 0.8–1.3[a] | 24.6 |
| Optical path length (m) | $3300 < L < 3450$[b] | 76 |
| Cell volume (L) | 0.4 | 0.5 |
| Cell pressure (kPa) | 19 | 8 |
| Sonic anemometer type | Gill Instruments R2A (3-D) | Gill Instruments HS (3-D) |
| Sample line inlet position | 0.25 m below sonic center | 0.25 m below sonic center |
| Sonic measurement height (m) | 1.2 | 1.2 |
| Sampling tube length (m) | 6.7 | 25 |
| Sample gas flow at inlet (slpm) | 30.5 | 13.5 |
| Selected data acquisition rate (Hz) | 20 | 8 |

[a] There are four closely spaced $CH_4$ absorption lines, which are not resolved by the FMA. [b] The exact value is not known. The lower limit was estimated based on normal operation condition of the FMA, i.e. measuring ≈2 ppm $CH_4$ at a cell pressure of 19 kPa results in about 16% absorption signal. This translates in 3.3 km considering the line intensities and assuming no optical loss within the cavity. The upper limit is calculated from the reported cavity ring-down time of 11.6 μs.

rather challenging to validate the retrieved EC flux data, because one cannot rely on a reference method, and $CH_4$ emissions of natural sources are often very small. Although the analyzers may give the correct mixing ratio under laboratory conditions, these readings do not necessarily translate to a representative surface fluxes during a field campaign.

Here we characterize and compare two cryogen-free optical analyzers that allow for fast and high precision measurement of methane mixing ratios in ambient air. For the validation of flux data during field deployment, an artificial methane flux was generated at the surface of an intensively managed grassland with otherwise very low methane flux. To our knowledge, this is the first example of an intercomparison for methane flux measurements where eddy covariance $CH_4$ flux data were validated against a known, artificial source.

## 2 Material and methods

### 2.1 Instrumentation

In this study, we investigated two commercially available optical analyzers that are cryogen-free and allow for $CH_4$ measurements at high (>10 Hz) temporal resolution: 1) an off-axis integrated-cavity output spectrometer (FMA, Fast Methane Analyzer, Model 908-0001, Los Gatos Research Inc., Mountain View, CA) and 2) a dual continuous-wave (cw) quantum cascade laser based direct absorption spectrometer (QCLAS, Model QCL-76-D, Aerodyne Research Inc., Billerica, MA). Even though the optical implementation and the signal processing techniques used in the two instruments are quite different, the underlying principles of infrared (IR) absorption spectroscopy apply to both analyzers. The trace gas mixing ratios are determined based on the Beer-Lambert law:

$$\ln(I_0/I) = k_\nu n L = S_i \phi_\nu n L \quad (1)$$

which relates the attenuation of light ($I$ and $I_0$ being the transmitted and incident light intensity, respectively) to the number density $n$ [molecule/$cm^3$] of absorbing molecules along the light path of length $L$ [cm]. In this equation $k_\nu$ [1/(molecule $cm^{-2}$)] denotes the spectral absorption coefficient for an isolated transition $i$, and it is defined by the line strength of the transition $S_i$ [$cm^{-1}$/(molecule $cm^{-2}$)] and by the normalized line shape function $\phi_\nu$ [1/$cm^{-1}$]. The number density, $n$, can easily be expressed in mole fraction of the absorbing species using the ideal gas law. Given that the minimum detectable mixing ratio is determined by the noise-equivalent-power, absorption path length, absorption cross-section and the incident laser power, it is evident that the detection sensitivity can be optimized using several approaches.

The QCLAS employs a mid-IR quantum cascade laser as light source which is particularly attractive due to its stable single mode spectral output, high power and near room temperature operating condition. The advantage of selecting the mid-IR spectral region is that the majority of trace gas molecules of interest have their fundamental ro-vibrational absorption bands located at these energies and therefore the absorption strengths are also the highest here. This explains the ability of the analyzer, equipped with two lasers, to measure not only $CH_4$ and $H_2O$, but also the mixing ratios of $N_2O$ and $NO_2$, respectively (see Table 1). For this study, however, only the $CH_4$ and $H_2O$ data were considered. The

signal-to-noise ratio is significantly improved by employing a multipass absorption cell which increases the effective light path through the absorber by more than two orders of magnitude. Nevertheless, the main challenge in the direct absorption approach is to accurately measure small changes ($\Delta I = I_0 - I$) of two large quantities. This limitation can be overcome by the rapid sweep integration technique, where the absorption spectrum is typically acquired at 5–10 kHz and the co-addition of many individual scans results in rapid gains in signal-to-noise ratio. Optical fringes mainly resulting from unwanted etalons formed by reflections and scattering in the multipass cell are effectively suppressed by a proper mechanical modulation of the cell's rear mirror using a piezo-crystal (McManus et al., 2006).

The FMA, on the other hand, operates in the near-IR region where low-cost distributed feedback diode laser sources as well as photodetectors with high detectivity values are readily available, and fibre optics can be efficiently used. This results in very compact, robust and easy-to-build systems. However, the absorption strength (overtone transitions) of the molecules is 10 to $10^3$ times weaker than in the mid-IR region. To circumvent this constraint, a high-finesse optical cavity with high reflectivity mirrors ($R > 0.9999$) is used to achieve an effective path length of light on the order of kilometers (see Table 1). Thus, the laser beam is trapped for tens of microseconds. The absorption signal is obtained in this case by the time integrated intensity of the light passing through the cavity with and without the absorbing medium and expressed as:

$$\Delta I / I_0 = GA/(1+GA) \quad (2)$$

where $A$ is the single-pass absorption [$A = 1 - \exp(-k_\nu d)$] and $G = R/(1-R)$. $R$ is the mirror reflectivity, and $d$ is the interaction length of the laser beam with the absorbing medium. Once the mirror reflectivity is determined from a known concentration standard, it also serves for the absolute calibration of the FMA.

For both analyzers, the absorption features are fitted to a Voigt profile, and the mixing ratios are retrieved based on measured pressure, temperature, path length and molecular parameters, which are listed in spectral data-bases such as HITRAN (Rothman et al., 2009). While the FMA is stated to be calibrated by the manufacturer, the QCLAS requires calibration by the user. More detailed descriptions of the instrumental design and signal processing have been published by Nelson et al. (2002) for QCLAS and by Baer et al. (2002) for FMA, respectively.

### 2.2 Measurement site

The field measurements were conducted at the Oensingen experimental site, which is located on the Swiss Plateau (7°44′ E, 47°17′ N) at an altitude of 450 m a.s.l. The managed grassland field is part of the global FLUXNET observation network and the two large integrated European projects CarboEurope and NitroEurope. The field is divided into two parts and they differ in the management intensity (Ammann et al., 2007). However, during the present experiment in spring, both fields were covered by similar short grass vegetation and did not show a significant methane exchange.

All experiments assessing the analyzers performance were performed in this field site, which was motivated by our effort to test the instruments under the same conditions as they are employed in the EC measurements. The only exception was the water dilution experiment, which required, as it will be discussed in Sect. 3.1.3, a temperature-controlled laboratory environment for an accurate water vapour generation and consecutive measurements by the analyzers.

### 2.3 Trace gas flux generation

An objective evaluation of the suitability and accuracy of the instruments for measuring methane fluxes by the EC method was achieved by an artificial flux generation system, which mimics an amplified ecosystem-atmosphere gas exchange. For this purpose, stainless steel tubing of 1/4″ outer diameter was used to construct a rectangular grid containing 30 flow orifices (30 µm, Lenox Laser, USA) as gas outlets. As illustrated in Fig. 1, the grid consisted of three parallel lines of 30 m length, 5 m apart to approximate a surface area of 300 $m^2$. Each line embodied 10 flow orifices placed every 3 m along the tubing to obtain an even release of trace gas across the fumigation area.

The gas release experiment took place in two periods between 25–29 March (south-westerly wind directions, see Fig. 1) and 30 March–6 April 2009 (north-easterly wind directions). For the first period, the trace gas was obtained through continuous dilution of pure $CH_4$ with $N_2$ to a concentration of 5%, while during the second period, a pressurized cylinder (40 L, Messer, Switzerland) containing 1% mole fraction of methane in pure $N_2$ was coupled to the manifold through a pressure regulator. The trace gas mixture was continuously released at a rate of 0.8 standard liters per minute (slpm) set by a mass flow controller (Vögtlin Instruments, Switzerland) at an overpressure of 182 kPa.

To relate the area of the artificial flux to the area seen by the measuring system, the footprint of the flux measurements was calculated according to Neftel et al. (2008). The calculations are based on the analytical footprint model by Kormann et al. (2001). The footprint density function of a flux sensor is determined using readily available data from the standard eddy covariance measurements. This footprint density function is then integrated over the fumigation source area given as quadrangular polygon (Fig. 1). Its fraction gives the dilution factor of the measured flux in relation to average emission flux in the source area. In some cases, the footprint was also influenced by the neighbouring extensive grassland field. This was, however, not problematic since both fields had similar short grass vegetation during the experiment in spring.

### 2.4 Flux measurements

During the field measurements, the FMA was placed in a weatherproof housing close to the eddy flux tower, whereas the QCLAS was kept in an air-conditioned (23±2 °C) trailer to minimize temperature fluctuations. Additionally, the entire optical module of the QCLAS was insulated and maintained at 35±0.1 °C. A constant flow of dry air purged the optics to prevent condensation, which may occur due to the low temperature (16 °C) of the cooling water used for the QCL (Alpes Lasers, Switzerland ) and the IR-detectors (VIGO System, Poland). The trailer was located about 25 m away from the eddy flux tower in crosswind direction. The instrument automatically switched between ambient air (four hours) and calibration gas (two minutes). The FMA ran without any calibration procedure.

For the flux measurements, each trace gas analyzer was connected to a separate sonic anemometer (with the air inlet 0.25 m below the center of the sonic head), thus forming two individual eddy flux systems (see Table 1). The two EC systems were mounted close to each other at a lateral distance of 0.7 m. In addition, $CO_2$ and $H_2O$ fluxes were routinely measured with another EC system on the same field (Ammann et al., 2007) positioned at a distance of about 7 m. In order to better match the overlap between the size of the flux footprint and the $CH_4$ fumigation area, the measurement height of the EC systems was chosen relatively low at 1.2 m above ground.

For the EC flux measurements, the FMA was connected to an external vacuum scroll pump (XDS-35i BOC, Edwards, UK) with a maximum pumping capacity of 580 lpm. The sample was drawn through 6.7 m long tubing (8 mm i.d.) followed by two serially mounted filters (5 µm and 0.3 µm, AFM Series, SMC Inc., Japan) with droplet separator. The FMA has a pressure controller that throttles the flow to maintain the cell at its target pressure of ≈19 kPa. Due to the pressure drop within the sampling system and analyzer, the pumping speed was reduced to an effective gas flow of about 30.5 slpm.

The QCLAS was connected to a scroll pump (TriScroll 600, Varian Inc., Italy) with a maximum pumping capacity of 420 lpm. As the QCLAS has no built-in pressure or flow control system, it is left to the user to deal with these issues. In the present study, a mass flow controller (Red-y Smart-Series, Vögtlin Instruments, Switzerland) regulated the gas flow into the absorption cell, while a high-flow throttle valve (SS-63TS8, Swagelok, USA) was used to provide manual control of the downstream flow to keep the cell pressure at about 8 kPa. Since the analyzer was placed in a trailer 25 m away from the eddy flux tower, a custom made PTFE sampling tube (6 mm i.d., Hot Tube, Clayborn Lab, USA) was used to conduct the air stream to the instrument. The air sample was first filtered at the inlet by a slightly heated Quartz filter (MK 360, Munktell Filter, Sweden) and secondly before entering the absorption cell using a 7 µm sintered metal filter (SS-4F-VCR-7, Swagelok, USA). The sampling tubing was maintained at about 10 °C above ambient temperature by applying a constant current through its heating elements. The air was dried using a Nafion drier (PD-100T, Perma Pure, USA) just before the analyzer. This setup resulted in a turbulent flow of 13.5 slpm.

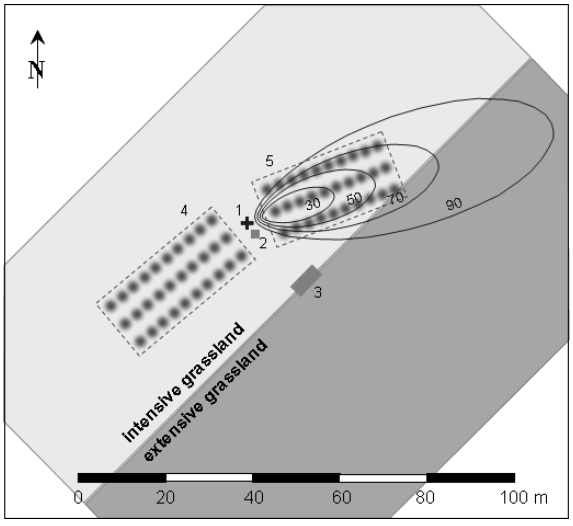


**Fig. 1.** Schematic map of the experimental field setup. (1) position of both EC flux systems: sonic anemometers and sample tube inlets for QCLAS and FMA; (2) weatherproof housing with the FMA; (3) trailer housing the QCLAS; (4) and (5) alternate positions of fumigation grids for the two main wind directions: circles indicate the position of the 30 release orifices, the dashed enveloping rectangle represents the source area used in the footprint calculation (assuming a constant average emission flux). The contour lines illustrate the flux footprint with 30%, 50%, 70%, and 90% flux contribution for a northeasterly wind case on 31 March 2009 11:00–14:30 CEST ($u$=3.8 m s$^{-1}$, $z/L$=−0.1).

More details about the EC setups and data processing methods are given by Eugster and Plüss (2010) and Neftel et al. (2010) for the FMA and QCLAS setup, respectively. In contrast to Eugster and Plüss (2010), the methane signal of the FMA system was linearly detrended prior to the flux calculations to be consistent with the data processing strategy of the QCLAS EC system.

## 3 Results and discussion

In this section, we first present the results of the analyzers' performance tests and discuss the various effects which may influence the retrieved mixing ratio values. Then, in situ methane mixing ratio measurements and $CH_4$ flux determination of the artificially fumigated area will be discussed. Finally, we compare the experimentally determined fluxes with the known emissions of the fumigation area.

### 3.1 Instrument characterisation

#### 3.1.1 Precision

The instrument performance in terms of detection limit and stability over time was characterized in the field by the Allan variance technique (Werle et al., 1993). For this purpose, the analyzers were connected through a T-split to a pressurized air cylinder and they measured the same dry gas over 16 h. The gas flow rate was 2 slpm and the analyzers were configured for low flow mode, but maintaining the same cell pressure as in the high-flow mode used for EC measurements (see Table 1). The total gas consumption of the analyzers was 1.28 slpm, while the rest was released through an overflow. The methane mixing ratio was measured with a time resolution of one second. The precision was 1 and 3 ppb $Hz^{-1/2}$ for FMA and QCLAS, respectively (Fig. 2). From the associated Allan variance plots an optimum averaging time on the order of 500 s can be derived. This corresponds to a detection precision of 0.23 and 0.58 ppb, respectively. For integration times beyond 500 s, the Allan variance levels off and even increases, which indicates the presence of $1/f$-type and "drift" noise. It is noteworthy that the Allan variance may have significant variations in time. This behaviour is indicated in Fig. 2 where the range defined by many individual 30 min Allan plots is shown (shaded area). Such representation illustrates that it is always possible to obtain "nice" Allan plots with low drift, and hence good precision, by selecting the best data segment from an extended time series. Figure 2 also shows that for half hour averaging (commonly used in EC techniques) the advantage of the FMA's higher short-time precision is somewhat diminished by low frequency instrumental drifts.

The Allan variance plots in Fig. 2 are typical in the sense that they contain frequency independent white noise and frequency dependent $1/f^{\alpha}$ ($\alpha>1$) noise (Werle et al., 1993). The latter encompasses a noise at low frequencies which can be considered as drift. Accordingly, the Allan variance has a characteristic "V-shape" defined by the white-noise dominated region at short integration times and by the domain of various drift effects at longer integration times. Our results are consistent with other recent work (Kroon et al., 2007; Smeets et al., 2009; Eugster and Plüss, 2010; Bowling et al., 2009), suggesting that the achievable detection limit for methane with the existing analyzers is about 1 to 5 ppb $Hz^{-1/2}$, which implies that variations of 0.05% in ambient methane mixing ratio are readily captured. The only strikingly different Allan variance plot has recently been published by Hendriks et al. (2008). This plot has no clear domains nor local minima, and the reported precision ($6.1\times10^{-3}$ ppb $Hz^{-1/2}$) is at least two orders of magnitude better than what is expected from the stated precision (4.74 ppb) at a sampling rate of 10 Hz. Assuming a pure white-noise behaviour of the analyzer, the estimated precision should rather be $4.74/\sqrt{10}$ or 1.5 ppb $Hz^{-1/2}$.

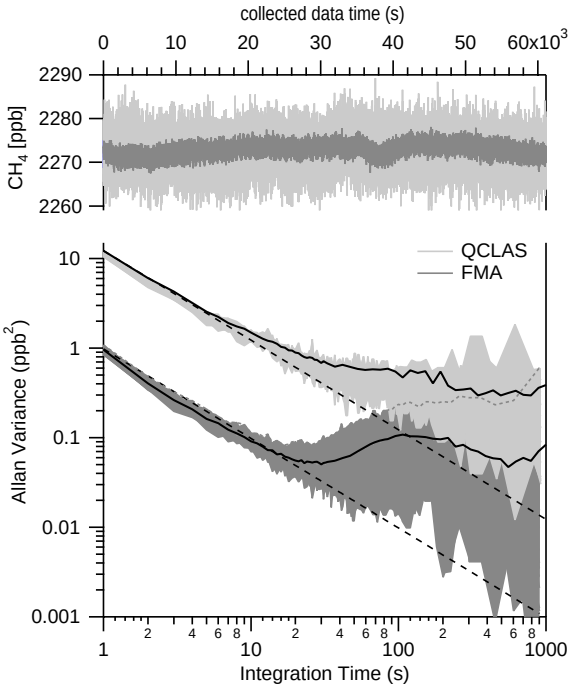


**Fig. 2.** Precision and stability over time of both analyzers quantified by the Allan variance technique. The top part shows the $CH_4$ mixing ratio measured over 16 h by the two analyzers from a pressurized air cylinder. Data from the QCLAS are shown in light gray, those from the FMA are in dark gray. The bottom part is the log-log plot of the sample variance as a function of the averaging time. The dashed line indicates the white-noise behavior, while the black line is the variance associated to the long-term measurement. The time series was also split into 30 min sequences and all individual Allan variance plots were calculated. The filled areas thus represent the envelope of all individual 30 min Allan variance plots, indicating the range that typical 30 min Allan variances would fall into.

#### 3.1.2 Accuracy

In principle, direct absorption spectroscopy is an absolute method that should allow for a straightforward calculation of the mixing ratio from the measured signals. However, the accuracy of this calculation depends on the knowledge of the molecular line parameters including line strength, pressure and temperature dependence (listed in the spectral databases), as well as instrumental laser line width and shape. Additionally, non-unity gain factors and potential pressure broadening effects also bias the retrieved mixing ratios. Whereas the FMA is delivered with factory calibration, the QCLAS is shipped without calibration, and all corrections need to be performed by the user during a post processing step.

Three reference gases were used to determine the accuracy and the linearity of the analyzers and to calibrate the QCLAS. One cylinder (1838.5±0.3 ppb $CH_4$) was prepared and calibrated at the World Meteorological Organization (WMO)

Central Calibration Laboratory (CCL), while the other two (2273.1±0.5 ppb and 2478.8±0.5 ppb, respectively) were secondary standards linked to the WMO mole fraction scale. A four-point calibration (including zero) was performed, but given the stability and linearity of the analyzers a two point calibration would be sufficient. The calibration factor was 1.0003 and 1.0516 for FMA and QCLAS, respectively. The reproducibility determined by replicate measurements of the target tank was 0.9 ppb for FMA and 1.7 ppb for the QCLAS. It is noteworthy that the excellent accuracy of the FMA has been maintained even after transport and under field deployment.

#### 3.1.3 Response to water vapour

It is well known that density fluctuations arising from heat and water vapour fluxes affect the measured flux densities of trace gases according to the Webb-Pearman-Leuning (WPL) theory (Webb et al., 1980). The following paragraphs are dealing with considerations related to water vapour that are not directly covered by the WPL theory, such as the effect of water vapour on the spectral line shape. Drying the air sample or measuring its absolute moisture content is required for an accurate methane mole fraction determination. This is, because the laser spectrometers measure the mixing ratio of $CH_4$ to total pressure ($P_t$), including also the vapour partial pressure ($P_w$=[$H_2O$]$P_t$), whereas the methane mixing ratio in calibration gas is defined as *dry air mole fraction*. A dilution correction must thus be applied to the reported raw mixing ratio values

$$[CH_4]_{dry}=[CH_4]_{wet}\,P_t/(P_t-P_w) \quad (3)$$

Furthermore, changing the gas composition by varying its water content will influence the spectral line shape of the absorbing molecule (in this case $CH_4$) due to the collisional broadening effect and thus, the derived mixing ratio value. As the line shape function (see Eq. 1) is determined by the physical mechanisms that perturb the energy levels of the transition (Varghese and Hanson, 1984), it is obvious that perturbations caused by molecular collisions may differ as a function of the colliding molecules type. Within the binary collision assumption the collisional broadening effect is introduced as a Lorentz function with a full-width at half maximum ($\gamma_c$) that is proportional to the sample pressure

$$\gamma_c = \sum_j \gamma_j P_j \quad (4)$$

where $\gamma_j$ ($cm^{-1}\,atm^{-1}$) is the transition dependent broadening coefficient quantifying the ability of a molecular species $j$ (e.g. $N_2$, $O_2$, and $H_2O$) from the air sample to cause pressure broadening due to the collisions with the absorbing molecules. The role of this collision-induced interference of spectral lines in ro-vibrational spectroscopy is in many cases underestimated. It is often stated that the instruments are interference free, which, however, only means that there is no spectral overlap between the absorption line of the trace gas of interest and the absorption features of other molecular species. Therefore, one might misleadingly assume that there is no cross-sensitivity to other ambient air species. Nevertheless, this assumption should be investigated carefully in the case of trace gas flux measurements, because water vapour concentrations can vary rapidly and are often correlated with vertical wind speed. Thus, any cross-sensitivity of trace gases to water may lead to an apparent flux. In principle, it would be possible to implement in the retrieval software an algorithm to account for this collision-induced effect based on the theory of pressure broadening. However, the commonly used spectral database, HITRAN, contains only the dry air broadened half-width ($\gamma_{air}$) for most of the absorption lines (Brown et al., 2003). Investigations performed on simulated spectra which included the pressure broadening effect showed that quantification using least-square fit of a Voigt profile will systematically underestimate the mixing ratio values. For ambient water vapour levels (<4%v), the magnitude of this underestimation can be well approximated using a linear dependence on the vapour partial pressure, and thus a simple cross-sensitivity correction can be applied to the measured $CH_4$ mixing ratio:

$$[CH_4]=[CH_4]_{dry}+b_{ct}P_w/P_t \quad (5)$$

where $b_{ct}$ is the cross-sensitivity coefficient of the particular device (Neftel et al., 2010), which can also be determined empirically as shown below. Before doing so, we should mention an important aspect regarding the above corrections. While the dilution effect depends only on the absolute amount of water vapour in the air sample, i.e. it is always present in humid air sample, the water pressure broadening causing the cross-sensitivity effect will depend linearly on the mixing ratio of the absorbing trace gas. This has an impact on the determination of the $b_{ct}$ value. For example, the slope will be twice as steep when the mixing ratio of the absorbing trace gas is doubled, but it vanishes as the mixing ratio approaches zero.

To investigate the effect of increasing humidity on the retrieved $CH_4$ mixing ratio, the analyzers were installed in an air conditioned laboratory and measured the gas from a pressurized dry air cylinder coupled to a water vapour generation system (LI-610, LI-COR Inc., USA). This dew-point generator gradually increased the humidity level of the gas every 20 min. The QCLAS simultaneously measured the methane mixing ratio and the water vapour in the humidified samples. Thus, every single $CH_4$ mixing ratio measurement can be normalized to dry conditions (see Eq. 3) given that the humidity data are calibrated. The LI-610 has been considered as reference point for absolute water concentration. The results of the water dilution experiment are shown in Fig. 3. It clearly indicates that correcting for dilution by water vapour only is not sufficient and, because no direct spectral interference to water vapour is expected in this spectral region, the

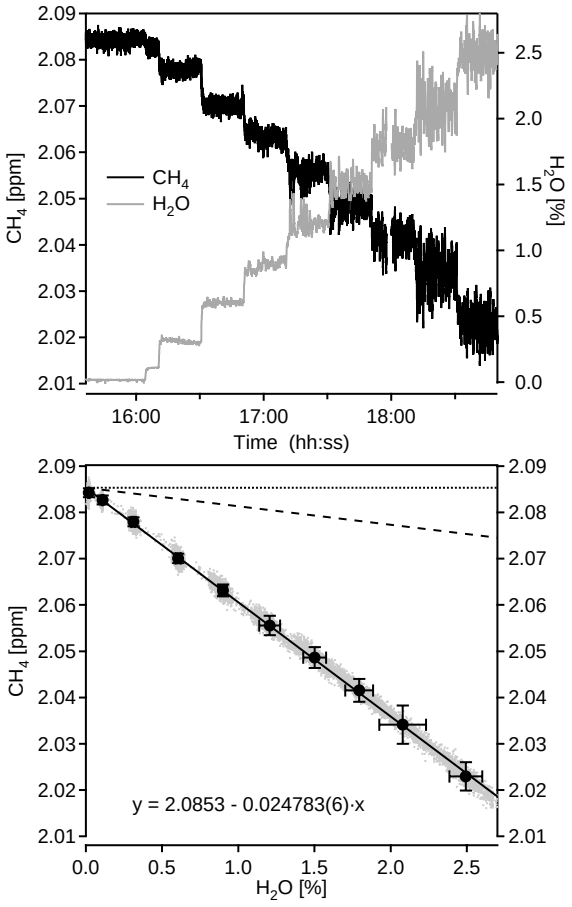


**Fig. 3.** Instrumental response to varying water vapor content. Top graph shows the methane mixing ratio changes measured by QCLAS over time induced by the stepwise addition of water vapour. The same behaviour was observed for both analyzers. The linear dependence of the $CH_4$ mixing ratio on the water vapour concentration as measured by QCLAS is indicated on the bottom graph. The gray dots show the original one-second data while the circles represent 20 min averages (with $1\sigma$ error bars) for the individual dilution steps. The solid line is a linear fit through the averaged data points. The dashed line indicates the apparent $CH_4$ mixing ratio after correction of the volumetric dilution (Eq. 3) by water vapor. The real (dry air) mixing ratio (dotted line) can only be obtained when an additional correction factor (Eq. 5) is applied to account for the pressure broadening effect.

observed behaviour is attributed to the line broadening effect of the increasing water content in the gas-matrix (Neftel et al., 2010). Moreover the effect shows, in accordance with the theoretical prediction, a clear dependence on the water vapour, which although is non-linear, it still can be approximated by a linear function at usual ambient water vapour concentrations (<4%v). In our case its magnitude is about 16% of the density correction, but as mentioned earlier, the exact value depends on the $CH_4$ mixing ratio as well as on the absorption lines which are used to retrieve the mixing ratios. In this context, it is rather a coincidence that both analyzers showed exactly the same cross-sensitivity effect, because the absorption lines analyzed by the instruments are located at different (near and mid-IR, respectively) spectral regions. In contrast to the QCLAS, the FMA measures a spectral feature of $CH_4$ that is a combination of four individual, but closely spaced, and thus not resolved, absorption lines (see Table 1). Nevertheless, this empirical approach allows for the determination of the cross-sensitivity coefficient $b_{ct}$ without the knowledge of the water pressure broadening coefficient value.

We also tried to repeat the dilution experiment in the field by gradually adding water vapour to the gas stream from a pressurized air cylinder as described by Neftel et al. (2010), but in this case the FMA showed only a random response to the increased humidity. One could only speculate about the nature of such behaviour. One possible source could be the presence of two serially mounted (5 µm and 0.3 µm) filters with droplet separators upstream of the FMA. These elements were used to further protect the cell mirrors during the campaign, but they may also have dampened the water vapor levels considerably. Since we had no means to determine the actual water content inside the cell of the FMA, the data interpretation became difficult.

To summarize, the dilution experiment gives us solid evidence that water vapour flux may introduce an apparent methane flux similar to the water vapour density effect. This is most significant for small $CH_4$ fluxes and large water vapour fluxes. In the density flux correction equation proposed by Webb et al. (1980) there are three terms:

$$F = \underbrace{\overline{w'\rho_c'}}_{\text{I}} + \underbrace{\mu\left(\overline{\rho_c}/\overline{\rho_a}\right)\overline{w'\rho_v'}}_{\text{II}} + \underbrace{(1+\mu\sigma)\left(\overline{\rho_c}/\overline{T}\right)\overline{w'T'}}_{\text{III}}, \qquad (6)$$

where $w$ is vertical wind speed in $\mathrm{m\,s^{-1}}$, $\rho_a$, $\rho_v$, and $\rho_c$ are the densities of air, water vapour, and a trace gas $c$, respectively, in $\mathrm{kg\,m^{-3}}$, $T$ is air temperature in K, and $\mu{=}m_a/m_v$ and $\sigma{=}\overline{\rho_v}/\overline{\rho_a}$. $m_a$ and $m_v$ are the molar masses ("weights") of dry air and water vapour, respectively, in $\mathrm{kg\,mol^{-1}}$. Term (I) is the measured flux, term (II) is the moisture flux correction, and term (III) is the sensible heat flux correction. Since temperature fluctuations are largely under control in a closed-path $CH_4$ analyzer such as the ones used here, this term becomes negligibly small and hence we will focus on term (II). This term is non-negligible if water vapour is not removed from the air stream prior to analysis or the measured mixing ratios are not individually corrected for the dilution effect. As shown by Neftel et al. (2010), the water cross-sensitivity on $CH_4$ can formally be treated similar to the density correction. Its influence increases linearly with the water flux and will consequently be most pronounced in summer conditions with high transpiration of the plant canopy. This effect is illustrated by a series of measurements over the same grassland field taken in August 2008, using the same QCLAS setup, but without drying the air samples. Consequently both, the

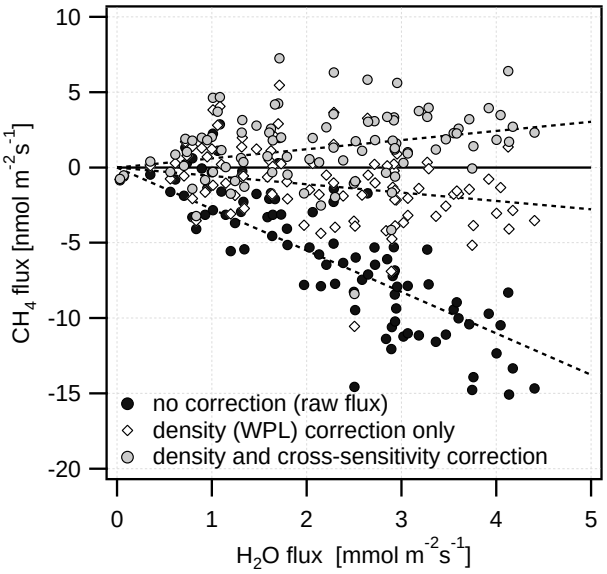


**Fig. 4.** Scatter plot of the evaluated $CH_4$ fluxes at different stages of corrections. These data were recorded with the QCLAS at the same site during August 2008 when water vapour fluxes were high and no significant methane fluxes were expected. The dashed lines show linear regression curves (forced through zero) for the three data-sets. The regression line slope for the data with "no correction" is $-2.7$ nmol $CH_4$ (mmol $H_2O$)$^{-1}$.

density (WPL) and the cross-sensitivity corrections had to be applied. This was performed numerically on the individual 20 Hz raw data values. This procedure avoids the potential overestimation of the correction due to the fact that the residence time of water molecules in the sampling line is slightly longer than that of non polar molecules such as $CH_4$ (Ibrom et al., 2007). Figure 4 shows the scatter plot of the evaluated $CH_4$ EC fluxes at different stages of corrections. The corrected fluxes have been evaluated with a prescribed lag that was derived from the maximum of the covariance function of the non corrected fluxes. This lag corresponds to the expected time delay based on the tube length, diameter and pump speed. The strong negative apparent $CH_4$ fluxes up to $-15$ nmol m$^{-2}$ s$^{-1}$ are evidently induced by water vapour fluxes, because the $CH_4$ exchange fluxes of the grassland system in Oensingen are expected to be very small. Applying the density correction reduces these negative fluxes by about a factor of 5. However, this still exceeds plausible limits of $CH_4$ uptake fluxes (Neftel et al., 2010; Smith et al., 2000). The second correction brings the $CH_4$ fluxes to slightly positive values that are individually not significantly different from zero, but do show a tendency to emission fluxes and positive correlation with the water vapour flux. These positive fluxes are on average higher than potential emissions from grassland vegetation reported by Keppler et al. (2006). Yet the results are strongly dominated by the uncertainties in the applied correction factors (water calibration of the QCLAS, cross interferences of the water vapour on the $CH_4$ mixing ratio) and are sensitive to any slight change in these factors.

Although not considered in this study, it should still be mentioned that an additional effect may also influence the final $CH_4$ flux values. This effect has its origin in the well known physical process of adsorption of gas molecules on solid surfaces predominantly due to attractive Van der Waals forces. In the classical model of gas adsorption (Langmuir's model) it is assumed that gas molecules striking the surface have a given probability of becoming adsorbed, while molecules already adsorbed similarly have a given probability of desorbing, which leads to a dynamic equilibrium where the average number of molecules per unit area of surface per time interval are constant. The accumulation of a specific molecule on a solid surface is influenced by many factors involved in the interactions between the solid surface, water and the species concerned. This also means that there is a possibility that trace gases like $CH_4$ could be influenced by changes in the air humidity due to the competitive sorption of water vapour on the surface. Given that water molecules have a high potential to replace other molecules from surfaces and variation in the water vapour concentrations in high flux conditions are on the order of 10%, i.e. about 5 orders of magnitude higher than the expected $CH_4$ variations, it may be worthwhile to consider this effect in future investigations.

### 3.1.4 Influence of temperature

The QCLAS is rather sensitive to ambient temperature fluctuations. This is due to the relative large number of optical elements and the thermoelectrically cooled (TEC) infrared detectors (Vigo Systems, PL). As mentioned in Sect. 2.1, the signal-to-noise ratio can be strongly influenced by optical fringes whose magnitude mainly depends on the alignment accuracy of the optical system. Furthermore, the employed detectors are particularly sensitive to the aiming angle of incident light. This is due to the small size of the photodiodes (0.5 mm$^2$ active area) and to their optical immersion into high refractive index GaAs hyperhemispherical lenses. The influence of the changes in the optical aiming on the measured $CH_4$ mixing ratio was empirically estimated by deliberately creating a misalignment which caused 5% decrease in the laser intensity on the detector. This resulted in an apparent change of 23 ppb $CH_4$. Considering the laser intensity variations of about 0.35% over many hours during the field campaign, the noise contribution to the analyzer precision was about 1.6 ppb at most.

The influence of changing cell temperature and pressure on the measured methane mixing ratio by FMA has also been investigated. Even though the analyzer showed an excellent stability during the field test, it was not completely immune to changes in ambient conditions and a temperature dependence of 0.84 ppb K$^{-1}$ could be established. Additionally, the $CH_4$ mixing ratio values systematically dropped by

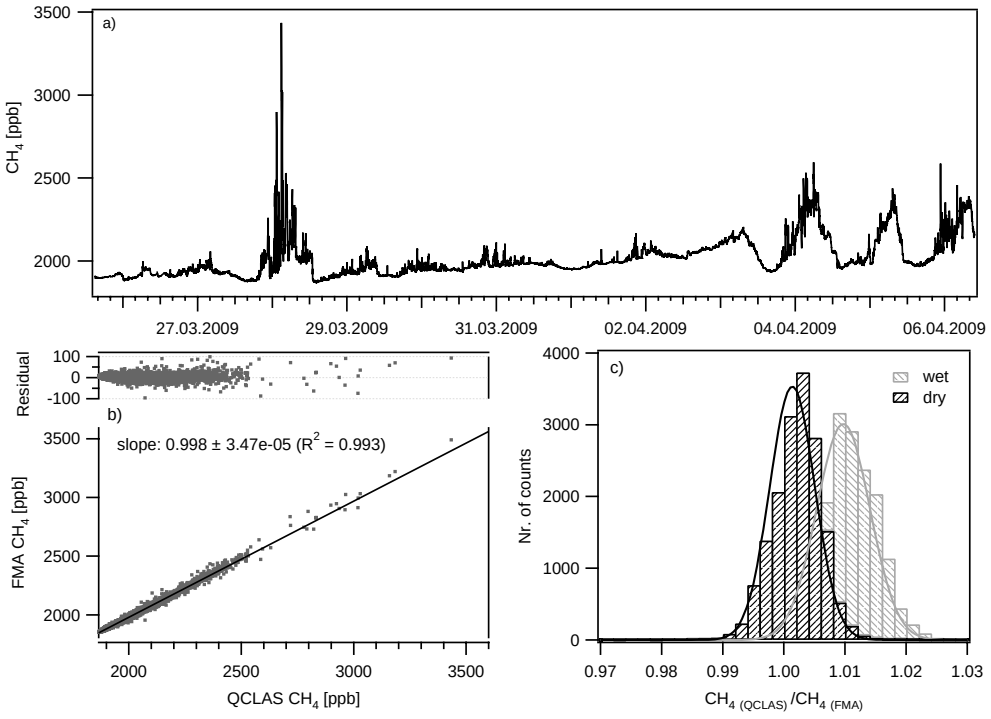


**Fig. 5. (a)** Time series of the methane mixing ratios during the field campaign measured by QCLAS. **(b)** Scatter plot between the data sets measured by QCLAS and FMA, and **(c)** a histogram plot of the ratio between these two data sets illustrating two situations: the ratio calculated using $CH_4$ measured by the FMA in humid air (gray bars) and the ratio when the FMA data were dilution corrected (black bars). The appended gaussian fit indicates that the ratio between the two data sets has a nearly normal distribution.

51 ppb when switching from low to high flow mode. This, however, has no influence on typical eddy covariance measurements.

As a concluding remark, the QCLAS is more sensitive to temperature fluctuations than the FMA. However, under well controlled environment this dependence can be efficiently suppressed. For both setups, the drifts due to ambient temperature changes are too slow to have any significant impact on EC flux measurements, but they are likely to affect accuracy of absolute mixing ratio measurements in case of long-term monitoring applications.

### 3.1.5 Response time

In order to evaluate their responsiveness, the analyzers were placed in the field in their typical sampling configuration as used for the eddy-covariance flux measurements. The FMA sample gas flow of about 30.5 slpm corresponds to 165 lpm gas flow at a nominal cell pressure of 19 kPa. Thus, the cell volume of 0.408 L is refreshed at approximately every 0.15 s. In this configuration the data acquisition was set to 20 Hz. For the QCLAS system, the sample flow of 13.5 slpm corresponds to 171 lpm at a nominal cell pressure of 8 kPa. Thus, the cell volume of 0.5 L is refreshed at approximately every 0.18 s. To be consistent with this physical response time, the spectral retrieval rate was set to 8 Hz, although data acquisition rates of up to 20 Hz would have been possible.

The above reported values for the cell refresh rate were calculated based on the cell volume divided by the actual pumping speed. The real response time (first order, $1/e$) was also empirically determined in the field, through the entire sampling setup, by rapidly switching from ambient air to calibration gas and fitting the rising/falling tail to an exponential function. The instrumental response (0.23 s for QCLAS and 0.4 s for FMA) of this empirical approach is slightly slower than expected based on the well-mixed reactor model. This can be explained by the presence of filter and drier elements in the sampling system which may cause some smearing. This is consistent with the cut-off frequency of about 2 Hz in the cospectra.

In summary, the response time of both setups was slightly longer than expected from the manufacturers' specifications, which typically consider the cell volume and the sample flow. However, since this parameter is properly taken into account by the dampening correction, it does not pose any significant limitation on the flux measurements.

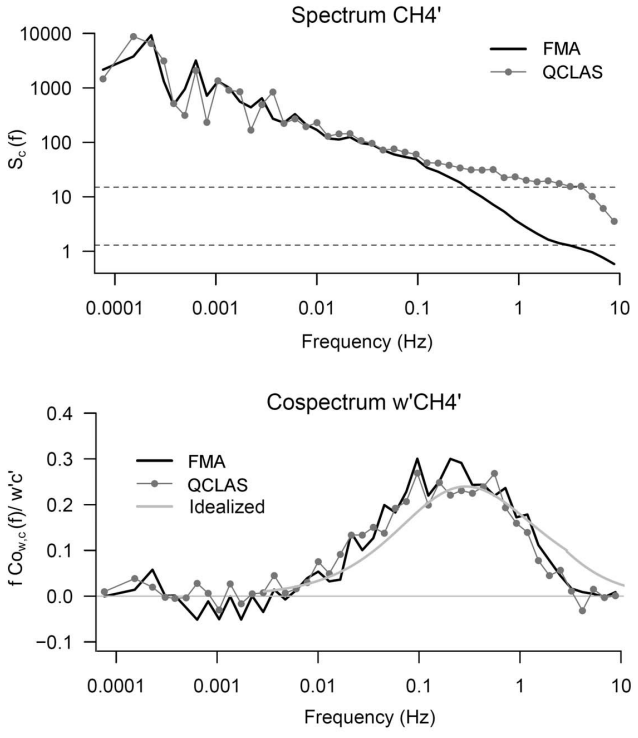


**Fig. 6.** Comparison of spectra and cospectra during high flux conditions (102 nmol $CH_4$ $m^{-2}$ $s^{-1}$, 31 March 2009, 11:00–14:38 CEST (218 records) with $u$=3.86 m $s^{-1}$). The gray line shows the idealized cospectrum for neutral and unstable conditions according to Kaimal et al. (1972).

### 3.2 $CH_4$ mixing ratio and fluxes

Time series of the methane mixing ratios during the field campaign are shown in Fig. 5. The $CH_4$ mole fraction values retrieved by the QCLAS were averaged to 1 min, calibrated and reported in dry air. The comparison of the data sets obtained from the two instruments is illustrated by a scatter plot with the associated histogram of their ratio. The combined effect of water dilution and pressure broadening experienced by the FMA led to a shifted and broadened distribution profile of the histogram. This is because contrary to the FMA which directly measured $CH_4$ in humid air samples, the strategy for the QCLAS measurements was to dry the air. Nevertheless, available air humidity measurements at the site allowed for an approximate correction of water effects on the methane mole fraction values measured by the FMA. It is evident that not drying the air only led to about 1% error at most in absolute mixing ratio during the entire field campaign, which is acceptable for most applications if only methane mixing ratios have to be measured, but not for EC flux measurements without appropriate corrections.

The excellent agreement of both analyzers for mixing ratios does not automatically imply comparable results with respect to flux measurements. Thus, we have also tested whether (i) the sensitivity of the two $CH_4$ analyzers is sufficient to resolve the artificial flux produced by fumigation from a rectangular surface and (ii) the calculated flux agrees with the flux value estimated based on the applied emission rates.

Figure 6 shows cospectra and power spectra obtained during a period with high artificial $CH_4$ flux (102 nmol $CH_4$ $m^{-2}$ $s^{-1}$). Since the two instruments gave very consistent results during the entire field campaign, these spectra can be considered as representative for our setups under stationary turbulence conditions. Contrary to the ideal Kaimal spectra, real spectra show systematic damping in the high frequency part, which must be corrected. For the QCLAS system, an empirical approach described by Ammann et al. (2006) was used. This correction can be parameterized as a function of the wind speed and will be specific to the used set-up. For the FMA system, the correction was derived from the damped cospectra which are approximated by a statistical best fitted theoretical cospectra as suggested by Eugster and Senn (1995). The difference between the two methods was analyzed and quantified by calculating the damping loss correction for the QCLAS with the same approach as for the FMA. This would lead to an average reduction of correction of about 6% for the QCLAS EC-system.

The agreement of measured cospectra with the idealized Kaimal cospectra (Kaimal et al., 1972, with minor modifications as shown by Eugster and Senn, 1995) is remarkable for both instruments, despite the larger noise level of the QCLAS (see Fig. 6). It is also noteworthy, that the significantly larger white noise level of the QCLAS does not compromise its performance for flux measurements. This is not unexpected since the eddy covariance method is a random-noise rejection method, that is, because random noise of the $CH_4$ sensor is uncorrelated with random noise of the wind sensor, the covariances and thus the cospectra are unaffected by pure random noise. What is however clearly seen is the fact that both systems are not perfect at the highest frequencies and the cospectra differ from idealized conditions as expected from first-order damping (Eugster and Senn, 1995).

The main goal of the fumigation experiment was to investigate whether the EC systems adequately measure the simulated flux. Therefore, the calculated 30-min fluxes were compared to each other as well as against the fumigation flux (see Fig. 7). In order to compare the measured fluxes with the emissions from the fumigation area, the footprint correction according to Neftel et al. (2008) was applied. This correction was calculated for each system individually, as the towers were slightly apart from each other (0.7 m). Yet the footprint correction factors for the two flux systems differed mostly by less than 10%. Periods with less than 20% contribution from the artificial source were not included in further analysis because the uncertainties inherent to the footprint calculation were considered as too large. The agreement between the footprint corrected fluxes and the released trace gas flux was remarkable and even fluctuations in the flux due to changes

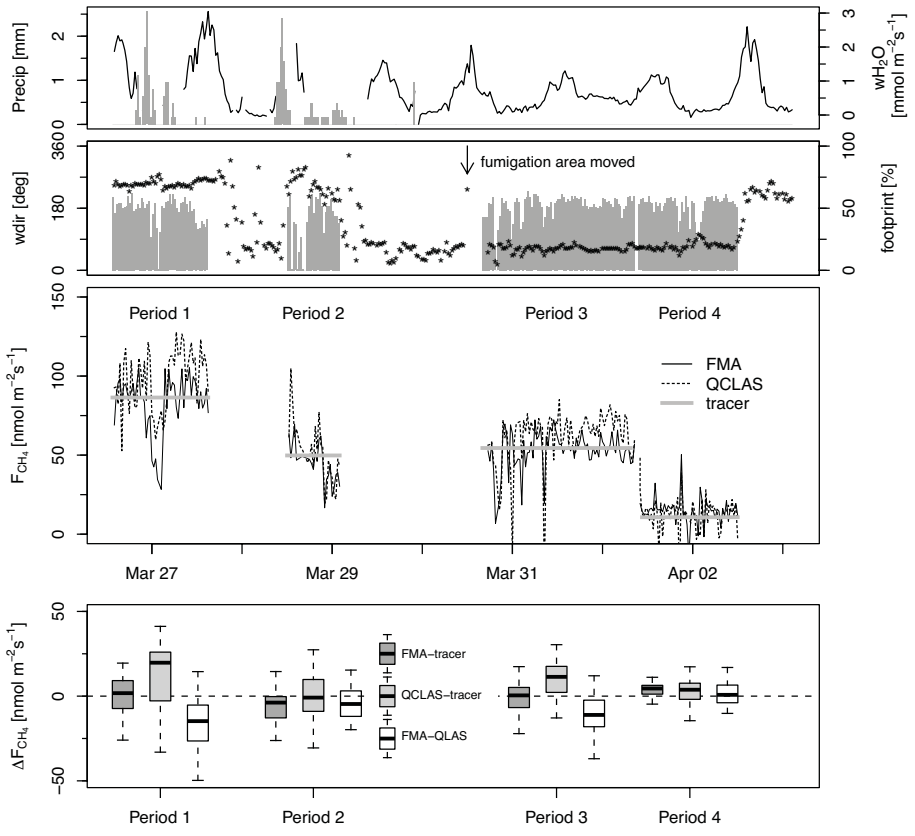


**Fig. 7.** Methane fluxes during the fumigation experiment. The top panel shows precipitation and the water vapour flux. Wind direction and the proportion contributed by the fumigated area to the measured flux are displayed in the second panel. In the third panel, the footprint corrected fluxes are plotted for the fumigation periods. The gray solid line represents the applied flux. Additionally, the boxplot illustrates the difference of the measured and the applied flux for each system as well as the difference between the two instruments for each fumigation period. The upper and lower ends of the box are drawn at the quartiles, and the bar through the box at the median. The whiskers extend from the quartiles ± 1.5 the inter quartile range.

in wind direction occured simultaneously. Nevertheless, the agreement with the known source was poor during these conditions, because the sudden shifts in wind direction might not be reflected precisely enough by the footprint calculated with half-hourly averaged micrometeorological quantities. As soon as the wind direction was constant, the scatter of the measured and footprint weighted fluxes was getting very small. The methane flux measured by the QCLAS system was systematically slightly higher than the flux determined based on the FMA measurements. However, the mean difference was 5.9 nmol $CH_4$ $m^{-2}$ $s^{-1}$ and thus well below the uncertainty that one would expect for eddy covariance flux measurements. This is remarkable given that the relevant data included not only mixing ratio measurements but also all assumptions and procedures used during flux calculation and the relevant footprint simulation.

We also recall that during the field campaign the sample was dried for QCLAS measurements, whereas the FMA was analyzing humid air. Thus, for an unbiased comparison, the methane flux retrieved by the FMA system had to be corrected for density fluctuations (WPL term) as well as for cross-sensitivity effect according to the approach of Neftel et al. (2010). For illustration, we calculated term II of Eq. (6) for typical conditions experienced during our experiments. Taking for the water flux $w'\rho_v'$=4 mmol $m^{-2}$ $s^{-1}$, the average methane mixing ratio [$CH_4$]=2 ppm (from Fig. 5) and the water effect quantified by the dilution experiment (from Fig. 3), the term II results in a flux of 5.6 nmol $m^{-2}$ $s^{-1}$. This conservative estimate shows that the resulting correction is relatively small in our case compared to the large, artificially issued flux of 84 nmol $m^{-2}$ $s^{-1}$ (see Fig. 7). Under certain conditions – especially for high water vapour fluxes combined with low methane fluxes – the WPL and cross-sensitivity corrections might well dominate the flux measurements as has been shown by Neftel et al. (2010) for background $N_2O$ flux measurements.

## 4 Conclusions

This paper demonstrates the benefits of using infrared laser absorption spectroscopy for in situ, fast and high precision ambient methane mixing ratio measurements. The compact and cryogen-free instruments can be operated unattended in the field to provide continuous measurements of $CH_4$ mixing ratios. Their fast response provides the opportunity to investigate the temporal dynamics of the mechanisms controlling ecosystem-atmosphere $CH_4$ exchange. Overall, both systems are performing remarkably well for flux measurements. To our knowledge, this is the first example of an intercomparison of direct eddy covariance methane flux measurements and the first time that eddy covariance $CH_4$ flux data has been validated based on a known, artificial methane emission.

Detailed investigation of the instrumental response to various parameters revealed, in agreement with recent publications (Neftel et al., 2010; Chen et al., 2010), that infrared gas analyzers employing laser absorption techniques may show some response to the gas-matrix composition, especially to water vapour. The empirically found correlation of $CH_4$ mixing ratio with sample gas humidity is in accordance with the theoretical expectation of the additional pressure broadening effect induced by the water on the $CH_4$ absorption line. Therefore, it is suggested that for eddy covariance measurements of small fluxes such cross-sensitivity effects should be taken into consideration independently of the employed wavelength and spectroscopic technique if (1) the sample is not dried prior to analysis or (2) the corresponding corrections are not implemented in the retrieval algorithms.

Ecosystem research will certainly have high benefits of recent developments achieved in infrared laser and detector technologies. This is particularly true for the quantum cascade laser fabrication. The latest continuous-wave (cw) QCLs can operate at room-temperature (up to 50° C) and have much higher output power and, thus, they are expected to allow significant improvements in the sensitivity of both direct absorption and cavity enhanced spectroscopy. It is also noteworthy, that the QCLAS used in this study simultaneously detects $N_2O$ and $NO_2$ with sufficient precision and time resolution for eddy covariance flux measurements. Similarly, the most recent cavity enhanced analyzers include multiple species, e.g. $CH_4$, $CO_2$ and $H_2O$, and perform dilution and line-broadening correction on the retrieved mixing ratio values. Finally, for both QCLAS and FMA, new analyzers capable of carbon isotope specific on-line $CH_4$ measurement are under development.

*Acknowledgements.* BT thanks Albert Manninen for sharing the Matlab code to generate absorption spectra which include the water broadening contribution. This study was supported by the COST action 729 project "Assessment of nitrogen biosphere-atmosphere exchange based on novel quantum cascade laser technology" SBF Nr. C06.0017, and by the project MAIOLICA of the ETH Competence Center Environment and Sustainability (CCES).

Edited by: E. C. Apel

## References

Ammann, C., Brunner, A., Spirig, C., and Neftel, A.: Technical note: Water vapour concentration and flux measurements with PTR-MS, Atmos. Chem. Phys., 6, 4643–4651, doi:10.5194/acp-6-4643-2006, 2006.

Ammann, C., Flechard, C. R., Leifeld, J., Neftel, A., and Fuhrer, J.: The carbon budget of newly established temperate grassland depends on management intensity, Agr. Ecosyst. Environ., 121, 5–20, doi:10.1016/j.agee.2006.12.002, 2007.

Baer, D. S., Paul, J. B., Gupta, M., and O'Keefe, A.: Sensitive absorption measurements in the near-infrared region using off-axis integrated-cavity-output spectroscopy, Appl. Phys. B, 75, 261–265, doi:10.1007/s00340-002-0971-z, 2002

Bain, W. G., Hutyra, L., Patterson, D. C., Bright, A. V., Daube, B. C., Munger, J. W., and Wofsy, S. C.: Wind-induced error in the measurement of soil respiration using closed dynamic chambers, Agr. Forest Meteorol., 131, 225–232, doi:10.1016/j.agrformet.2005.06.004, 2005.

Bartlett, K. B. and Harriss, R. C.: Review and assessment of methane emissions from wetlands, Chemosphere, 261(1–4), 261–320, doi:10.1016/0045-6535(93)90427-7, 1993.

Bowling, D. R., Miller, J. B., Rhodes, M. E., Burns, S. P., Monson, R. K., and Baer, D.: Soil, plant, and transport influences on methane in a subalpine forest under high ultraviolet irradiance, Biogeosciences, 6, 1311–1324, doi:10.5194/bg-6-1311-2009, 2009.

Brown, L. R., Benner, D. C., Champion, J. P., Devi, V. M., Fejard, L., Gamache, R. R., Gabard, T., Hilico, J. C., Lavorel, B., Loete, M., Mellau, G. C., Nikitin, A., Pine, A. S., Predoi-Cross, A., Rinsland, C. P., Robert, O., Sams, R. L., Smith, M. A. H., Tashkun, S. A., and Tyuterev, V. G.: Methane line parameters in HITRAN, J. Quant. Spectrosc. Ra., 82, 219–238, doi:10.1016/S0022-4073(03)00155-9, 2003.

Bubier, J. L. and Moore, T. R.: An ecological perspective on methane emissions from northern wetlands, Trends Ecol. Evol., 9, 460–464, doi:10.1016/0169-5347(94)90309-3, 1994.

Camarda, M., Gurrieri, S., and Valenza, M.: Effects of soil gas permeability and recirculation flux on soil $CO_2$ flux measurements performed using a closed dynamic accumulation chamber, Chem. Geol., 265, 387–393, doi:10.1016/j.chemgeo.2009.05.002, 2009.

Chen, H., Winderlich, J., Gerbig, C., Hoefer, A., Rella, C. W., Crosson, E. R., Van Pelt, A. D., Steinbach, J., Kolle, O., Beck, V., Daube, B. C., Gottlieb, E. W., Chow, V. Y., Santoni, G. W., and Wofsy, S. C.: High-accuracy continuous airborne measurements of greenhouse gases ($CO_2$ and $CH_4$) using the cavity ring-down spectroscopy (CRDS) technique, Atmos. Meas. Tech., 3, 375–386, doi:10.5194/amt-3-375-2010, 2010.

Eugster, W. and Plüss, P.: A fault-tolerant eddy covariance system for measuring $CH_4$ fluxes, Agr. Forest Meteorol., 150, 841–851, doi:10.1016/j.agrformet.2009.12.008, 2010.

Eugster, W. and Senn, W.: A cospectral correction model for measurement of turbulent $NO_2$ flux, Bound.-Lay. Meteorol., 74, 321–340, doi:10.1007/BF00712375, 1995.

Eugster, W., Zeyer, K., Zeeman, M., Michna, P., Zingg, A., Buchmann, N., and Emmenegger, L.: Methodical study of nitrous ox-

ide eddy covariance measurements using quantum cascade laser spectrometery over a Swiss forest, Biogeosciences, 4, 927–939, doi:10.5194/bg-4-927-2007, 2007.

Fowler, D., Hargreaves, K. J., Skiba, U., Milne, R., Zahniser, M. S., Moncrieff, J. B., Beverland, I. J., Gallagher, M. W., Ineson, P., Garland, J., and Johnson, C.: Measurements of $CH_4$ and $N_2O$ fluxes at the landscape scale using micrometeorological methods, Philos T. Roy. Soc. A, 351, 339–356, 1995.

Friborg, T., Christensen, T., and Søgaard, H.: Rapid response of greenhouse gas emission to early spring thaw in a subarctic mire as shown by micrometeorological techniques, Geophys. Res. Lett., 24, 3061–3064, doi:10.1029/97GL03024, 1997.

Hendriks, D. M. D., Dolman, A. J., van der Molen, M. K., and van Huissteden, J.: A compact and stable eddy covariance set-up for methane measurements using off-axis integrated cavity output spectroscopy, Atmos. Chem. Phys., 8, 431–443, doi:10.5194/acp-8-431-2008, 2008.

Ibrom, A., Dellwik, E., Flyvbjerg, H., Jensen, N. O., and Pilegaard, K.: Strong low-pass filtering effects on water vapour flux measurements with closed-path eddy correlation systems, Agr. Forest Meteorol., 147, 140–156, doi:10.1016/j.agrformet.2007.07.007, 2007.

Kaimal, J. C., Wyngaard, J. C., Izumi, Y., and Coté, O. R.: Spectral characteristics of surface-layer turbulence, Q. J. Roy. Meteorol. Soc., 98, 563–589, 1972.

Keppler, F., Hamilton, J. T. G., Braß, M., and Röckmann, T.: Methane emissions from terrestrial plants under aerobic conditions, Nature, 439, 187–191, doi:10.1038/nature04420, 2006.

Kormann, R., Müller, H., and Werle, P.: Eddy flux measurements of methane over the fen "Murnauer Moos", 11°11′ E, 47°39′ N, using a fast tunable diode laser spectrometer, Atmos. Environ., 35, 2533–2544, doi:10.1016/S1352-2310(00)00424-6, 2001.

Kroon, P. S., Hensen, A., Jonker, H. J. J., Zahniser, M. S., Van't Veen, W. H., and Vermeulen, A. T.: Suitability of quantum cascade laser spectroscopy for $CH_4$ and $N_2O$ eddy covariance flux measurements, Biogeosciences, 4, 715–728, doi:10.5194/bg-4-715-2007, 2007.

Matthias, A. D., Yarger, D. N., and Weinbeck, R. S.: A numerical evaluation of chamber methods for determining gas fluxes, Geophys. Res. Lett., 5, 765–768, 10.1029/GL005i009p00765, 1978.

McManus, J. B., Nelson, D. D., Herndon, S. C., Shorter, J. H., Zahniser, M. S., Blaser, S., Hvozdara, L., Muller, A., Giovannini, M., and Faist, J.: Comparison of cw and pulsed operation with a TE-cooled quantum cascade infrared laser for detection of nitric oxide at 1900 $cm^{-1}$, Appl. Phys. B, 85, 235–241, 2006.

Neftel, A., Flechard, C., Ammann, C., Conen, F., Emmenegger, L., and Zeyer, K.: Experimental assessment of $N_2O$ background fluxes in grassland systems, Tellus B, 59, 470–482, doi:10.1007/s00340-006-2407-7, 2007.

Neftel, A., Spirig, C., and Ammann, C.: Application and test of a simple tool for operational footprint evaluations, Environ. Pollut., 152, 644–652, doi:10.1016/j.envpol.2007.06.062, 2008.

Neftel, A., Ammann, C., Fischer, C., Spirig, C., Conen, F., Emmenegger, L., Tuzson, B., and Wahlen, S.: $N_2O$ exchange over managed grassland: application of a quantum cascade laser spectrometer for micrometeorological flux measurements, Agr. Forest Meteorol., 150, 775–785, doi:10.1016/j.agrformet.2009.07.013, 2010, special Issue on Eddy Covariance (EC) flux measurements of $CH_4$ and $N_2O$.

Nelson, D. D., Shorter, J. H., McManus, J. B., and Zahniser, M. S.: Sub-part-per-billion detection of nitric oxide in air using a thermoelectrically cooled mid-infrared quantum cascade laser spectrometer, Appl. Phys. B, 75, 343–350, doi:10.1007/s00340-002-0979-4, 2002.

Rothman, L. S., Gordon, I. E., Barbe, A., et al.: The HITRAN 2008 molecular spectroscopic database, J. Quant. Spectrosc. Rad., 110, 533–572, doi:10.1016/j.jqsrt.2009.02.013, 2009.

Smeets, C. J. P. P., Holzinger, R., Vigano, I., Goldstein, A. H., and Röckmann, T.: Eddy covariance methane measurements at a Ponderosa pine plantation in California, Atmos. Chem. Phys., 9, 8365–8375, doi:10.5194/acp-9-8365-2009, 2009.

Smith, K. A., Dobbie, K. E., Ball, B. C., Bakken, L. R., Sitaula, B. K., Hansen, S., Brumme, R., Borken, W., Christensen, S., Prieme, A., Fowler, D., Macdonald, J. A., Skiba, U., Klemedtsson, L., Kasimir-Klemedtsson, A., Degorska, A., and Orlanski, P.: Oxidation of atmospheric methane in Northern European soils, comparison with other ecosystems, and uncertainties in the global terrestrial sink, Glob. Change Biol., 6, 791–803, doi:10.1046/j.1365-2486.2000.00356, 2000.

Varghese, P. L. and Hanson, R. K.: Collisional narrowing effects on spectral line shapes measured at high resolution, Appl. Optics, 23, 2376–2385, doi:10.1364/AO.23.002376, 1984.

Verma, S. B., Ullman, F. G., Billesbach, D., Clement, R. J., Kim, J., and Verry, E. S.: Eddy correlation measurements of methane flux in a northern peatland ecosystem, Bound.-Lay. Meteorol., 58, 289–304, doi:10.1007/BF02033829, 1992.

Webb, E., Pearman, G., and Leuning, R.: Correction of flux measurements for density effects due to heat and water vapour transfer, Q. J. Roy. Meteorol. Soc., 106, 85–100, 1980.

Werle, P. and Kormann, R.: Fast chemical sensor for eddy-correlation measurements of methane emissions from rice paddy fields, Appl. Optics, 40, 846–858, doi:10.1364/AO.40.000846, 2001.

Werle, P., Mücke, R., and Slemr, F.: The limits of signal averaging in atmospheric trace-gas monitoring by tunable diode-laser absorption spectroscopy (TDLAS), Appl. Phys. B, 57, 131–139, doi:10.1007/BF00425997, 1993.